BOUNDARY LAYER GROWTH AND LAPSE RATE CHANGES DETERMINED BY LIDAR AND SURFACE HEAT FLUX IN SOFIA *

E. Donev,

Department of Meteorology, Faculty of Physics, Sofia University, Bulgaria

K. Zeller,

USDA Forest Service, Rocky Mountain Forest and Range Experiment Station, Fort Collins, Colorado, USA

St. Panchev

Department of Meteorology, Faculty of Physics, Sofia University, Bulgaria

and *I. Kolev*

Institute of Electronics, Bulgarian Academy of Sciences, Bulgaria

Reveived March 24, 1994; revised Septemper 6, 1994

ABSTRACT

In this study the results from a boundary layer experiment, conducted in autumn 1991 over a flat, build–up urban area in Southeast Sofia, together with some models for mixed layer growth rates are used to investigate the layered structure of the vertical atmospheric stability distribution in the Sofia Valley. Lidar measurements of aerosol layer heights and morning boundary layer development are combined with surface eddy correlation measurements of kinematic heat and moisture fluxes, profiles of temperature and humidity, wind speed and wind direction. A diagnostic method is presented for determining vertical lapse rates using surface meteorological measurements and lidar returns observed during the transition from nighttime stable stratification to daytime convective boundary layer after the sunrise.

Key words: convective boundary layer, lidar, heat flux, lapse rate

I. INTRODUCTION

Sofia is situated in a valley surrounded by mountains. Typically the mountains cause a block in geostrophic wind flow, hence air easily stagnates over the downwind valley as ventilating horizontal winds below the ridge height are very weak. Large quantities of air pollutants from urban, vehicular and industrial sources are frequently trapped in stagnated air above the cite. Relief can be provided by vertical mixing due to solar generated surface heating which drives the diurnal development of the mixing height or well–structured convective boundary layer (CBL). Under these conditions, the height of the CBL (h) and the intensity of the capping inversion ($\Delta\theta$) in turn determine the ability of the atmosphere to disperse air pollution. The diurnal development and destruction of vertical temperature inversions and their heights

* The research was supported by Bulgarian National Foundation "Science" and USDA Forest Service, Rocky Mountain Forest and Range Experiment Station, Fort Collins, Colorado, USA.

associated with the development of the daytime CBL are important parameters for forecasting pollution levels and ventilation in the Sofia Valley. The interaction between local dynamic (adjacent mountains) and thermic (radiative nocturnal cooling) factors during the formation of the stable nocturnal layer leads to a complex layered structure in the valley's morning vertical stability. Often two or three strong inversion layers are vertically stacked at sunrise. These layers are vertically connected with in between isothermal or weak stability layers. This nonlinear distribution of the morning vertical temperature gradient makes the time prediction of morning boundary–layer growth and transitions in response to the surface heating very difficult. The growth rate of the CBL strongly depends on the lapse rate above the mixing layer, which as stated in the case of Sofia Valley is nonuniform with the height. Hence the CBL growth rate is a complex time dependent function and the only way to predict or model the CBL is to know the lapse rate distribution in height and time. The purpose of this paper is to study vertical stability during the transition to a convective boundary layer using lidar observed mixed layer height and depth of the entrainment area (from vertical distributions of urban aerosols), surface flux measurements and basic entrainment equations.

The study of surface mixing layer growth and evolution has resulted in a large number of mixing height models. The simplest of these models treats the underlying CBL as an isentropic layer with a strong gradients or "jumps" in potential temperature and wind speed at the inversion cap or entrainment zone (EZ). For these models a linear vertical heat flux profile is used within the CBL. First models (zeroth–order) neglect Δh, the finite thickness of the capping inversion and admit step–like "jumps" and constant ratio between heat fluxes at the surface and at the top of the mixed layer (Lilly 1968; Tennekes 1973; Carson 1973). Later some investigators (Zilitinkevich 1975; Zeman and Tennekes 1977; Tennekes and Driedonks 1981) have used the turbulent kinetic energy (TKE) budget at h instead of the constant heat flux ratio. Deardorff (1979) introduced the effect of an entrainment process within the mixed to stable transition layer or interfacial layer of thickness $\Delta h = h_2 - h_0$, defined as the region of negative (downward) heat flux (Fig.1). The average interfacial layer may have significant vertical thickness and some authors defined this layer as the region of enhanced temperature gradient. The upper limit of this region usually coincides with the top of the region of negative (downward) heat flux (Arya and Byun 1987). However, it is not always true for the lower limits. Following Wyngaard (1983), Arya and Byun (1987) and Fernando (1986), here we define $\Delta h_2 = h_2 - h$ as the depth of the capping inversion and $\Delta h_1 = h - h_0$ as the depth of the intermediate layer between the capping inversion and the mixed layer with slight temperature gradient (Fernando 1986). The potential temperature growth between h_0 and h_2 is the sum of the small $\Delta\theta_1$ and the relatively large $\Delta\theta_2 = \gamma_i(h_2 - h)$, where γ_i is the average temperature gradient in the capping inversion.

Below we give a summary of the basic entrainment equations, a description of the data and the model verifications used to develop a simple diagnostic method for investigating vertical stability after sunrise.

II. BASIC EQUATIONS

In zeroth–order models the CBL growth rate is defined and predicted for the mean mixed layer height h, where the potential temperature admits step–like jump $\Delta\theta_0$, $\Delta\theta_2 = \Delta\theta_0 + \gamma_e(h_2 - h)$ and γ_e is the potential temperature gradient over h_2, where the vertical heat flux and its vertical derivative vanished and h_0 is the height where the heat flux changes from a positive to a

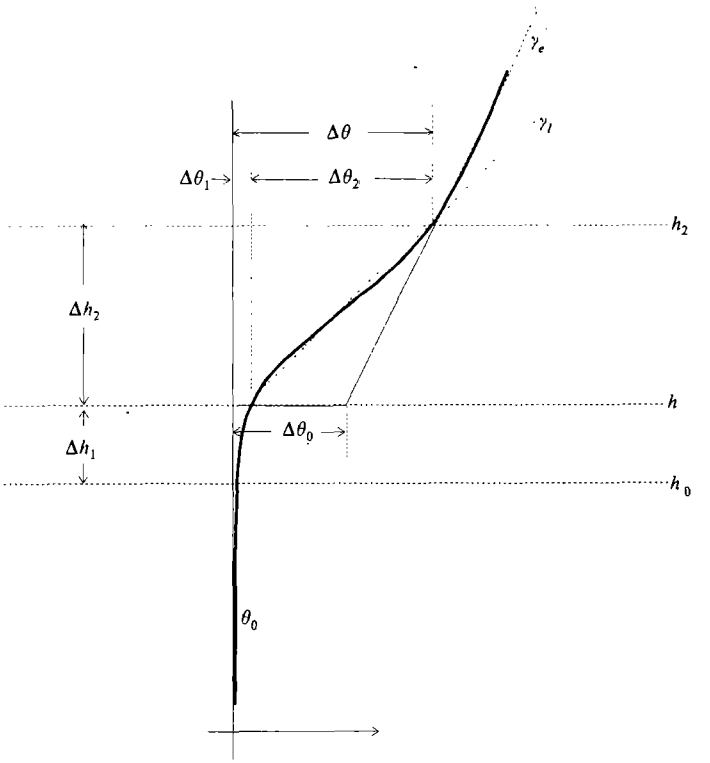

Fig. 1. Potential temperature as function of height in the entrainment zone.

negative value (Fig.1). If we neglect the small potential temperature gradient in the lower interfacial layer ($\Delta\theta_1 \approx 0$), we can use the simple zeroth–order models rate equations for the averaged mixed layer potential temperature $\Delta\theta_0$, the evolution of the step–like potential temperature jump $\Delta\theta_0$ and the growth of the mean mixed layer height (Tennekes 1973; Deardorff 1979). In all equations θ should be replaced by the virtual potential temperature θ_v to include moisture effects and the potential temperature flux by the virtual potential temperature flux $(\overline{w'\theta'_v}) = (\overline{w'\theta'}) + 0.61\theta_0(\overline{w'q'})$, where q is specific humidity and $(\overline{w'q'})$ is vapour flux.

The rate of change of $\Delta\theta_0$ is governed by the CBL growth rate and heating from the mixed layer below. Equilibrium between these two factors and the relative invariability of $\Delta\theta_0$ is assumed here (Deardorff 1980). Then

$$\frac{dh}{dt} - W = \frac{(\overline{w'\theta'})_s - (\overline{w'\theta'})_i}{\gamma_e h} = \frac{(\overline{w'\theta'})_s}{\gamma_e h_0}, \tag{1}$$

where $(\overline{w'\theta'})_s$, $(\overline{w'\theta'})_i$ and $(\overline{w'\theta'})_0 = 0$ are the heat fluxes at the surface, at the top of the mixed layer h and at h_0, W is the mean vertical velocity at h. The solution of these equations requires an assumption concerning the behaviour of heat flux $(\overline{w'\theta'})_i$ at the inversion base or an assumption for the ratio of h and h_0. There are two general approaches: vertical integration of the energy budget inside the mixed layer or parameterization of the local energy budget at the inversion base. The simplest suggestion is the constant heat–flux ratio (Tennekes 1973; Carson 1973)

$$(\overline{w'\theta'})_i = -A(\overline{w'\theta'})_s, \tag{2}$$

where $A = 0.2$ has been used by Tennekes (1973). There are many different models depending on which terms in the TKE budget equation are ignored and how the remaining terms are parameterized. If shear generation at surface and at the inversion base is not neglected (Boers et al. 1984)

$$\frac{\left(\frac{dh}{dt} - W\right)}{w_*} = \frac{A_1\left(\frac{w_m}{w_*}\right)}{\left[C_1 - D_1\left(\frac{\Delta u^2}{w_m^2}\right) + \frac{w_*^2}{w_m^2} Ri_1\right]}, \tag{3}$$

where $w_* = [gh(\overline{w'\theta'})_s / \theta_0]^{1/3}$ is the convective velocity and $Ri_1 = (gh\Delta\theta_0)/(\theta_0 w_*^2)$ is the convective Richardson number. If the dissipation term is included (Tennekes and Driedonks 1981)

$$\frac{\left(\frac{dh}{dt} - W\right)}{w_*} = \frac{A_2\left(\frac{w_m}{w_*}\right) - A'_2\left(\frac{Nh}{w_*}\right)}{\left[C_2 - D_2\left(\frac{\Delta u^2}{w_m^2}\right) + \frac{w_*^2}{w_m^2} Ri_1\right]}, \tag{4}$$

where N is the Brunt–Vaisalla buoyancy frequency, defined by $N^2 = (g\gamma_e)/\theta_0$. Both Eqs. (3) and (4) need an evaluation of $\Delta\theta_0$, and Eq. (3) does not explicitly contain the lapse rate over the capping inversion γ_e. In both Eqs. (3) and (4), w_m is the scaling velocity for vertical motions used by Driedonks (1982); $w_m^3 = w_*^3 + Bu_*^3$, where u_* is the friction velocity and $B =$ a constant.

There are different experimental estimations of the constants in the upper equations: Tennekes (1973) $A = 0.2$, $B = 2.5$; Boers and Eloranta (1985) under convective conditions $A_1 = 0.32$ and $C_1 = 0.75$; Zeman and Tennekes (1977) $A_2 = 0.5$, $C_2 = 3.55$ and $A_2' = 0.024$; Driedonks (1982) $A_1 = 0.2$ and $C_1 = 1.5$, $A_2 = 0.6$, $C_2 = 4.5$ and $A_2' = 0.03$; Arya and Byun (1987) using Deardorff's (1974) results estimated $C_2 = 2$ and $A_2 = 0.4$ under convective conditions. For the comparison between model predictions, Arya and Byun (1987) used $A_1 = 0.2$, $C_1 = 1.5$, $A_2 = 0.4$, $C_2 = 1.5$ and $A_2' = 0.02$.

Deardorff (1979) derived the equation for the rate of change of $\Delta\theta$

$$\frac{d(\Delta\theta)}{dt} = \gamma_e\left[\left(\frac{dh}{dt} - W_0\right) + \frac{d(\Delta h)}{dt} - (W_2 - W_0)\right] - \frac{(\overline{w'\theta'})_s}{h_0}, \tag{5}$$

where W_2 is the mean vertical velocity at the top of the capping inversion and W_0 is the mean vertical velocity at the bottom of the interfacial layer. Here is assumed that h_0 is the height where the heat flux changes from a positive to a negative value. Our definition does not ensure such strong demand and can be treated as a first approximation. By vertical integration of the averaged thermodynamic equation in the entrainment layer and substituting (5) Deardorff (1979) obtained

$$\Delta\theta = \frac{\alpha(1-Y)(\overline{w'\theta'})_s + \gamma_e \Delta h Y \dfrac{\partial h_2}{\partial t}}{\dfrac{\partial h_2}{\partial t} - Y\dfrac{\partial(\Delta h)}{\partial t}}, \tag{6}$$

where $\alpha = \Delta h / h_0$ and Y is the shape factor of the potential temperature profile in the entrainment zone $Y = (1/\Delta h)\int_{h_0}^{h_2} f(z)\mathrm{d}z$, where $\theta(z) = \theta_0 + f(z)\Delta\theta, f_0 = 0 \leqslant f \leqslant 1 = f_2$. We suggest the approximation $Y = 0.5(1 - \Delta h_1 / \Delta h)$. We will employ Eqs. (1) and (6) to obtain γ_e and $\Delta\theta$ (in case of measured h_0 and h_2), some experimental data to verify γ_e and $\Delta\theta$ and Eqs. (3) and (4) to test the obtained γ_e and $\Delta\theta$.

III. EXPERIMENTAL DATA

In this paper we use two separate data sets of simultaneous measurements of h_0, h_2 (as the approximate heights of the base and the top of the capping inversion) and the surface heat flux $(\overline{w'\theta'})_s$ on days with clear, calm conditions which result in higher pollution levels. Additionally, several vertical temperature soundings are used. The observational periods with complete data sets are 0700—1300 LST on both 21 September and 11 October 1991. During these two days the surface turbulent fluxes were measured continuously throughout the day however lidar measurements were only taken during the period of 0700—1300 LST. These data allow us to compare lidar measured CBL heights and surface heat fluxes in the case of calm wind and clear air convective conditions over an urban area within a valley. Both data sets were collected from the Institute of Electronics, Bulgarian Academy of Sciences and the Dept. of Meteorology, Sofia University grounds in South Central Sofia within 300 m of each other.

1. *Meteorological Conditions*

Stagnation conditions predominated on 21 September. Early morning the Sofia area was under the influence of an anticyclone. After 1000 LST, a cyclone centred far in the north, began to weaken the anticyclone over Sofia. On 11 October West Bulgaria bordered the edge of an anticyclone centred over Romania. Sofia winds were calm however there were stratified clouds associated with the inversion layers. The effect of these clouds is not handled by our method and hence we see a larger deviation of measured compared to model heights on October 11 compared to the results on 21 September. Typically in the Sofia Valley before sunrise on stagnation days there is a strong temperature inversion near surface. The inversion base averages about 150 m high in early September and diminishes to about 50 m by late November (Donev et al. 1992a; 1992b) (Note the strong surface layer nocturnal radiation inversion is not included in this multilayer inversion classification). There is one or more inversion layers stacked vertically in height up to the top of the previous day's CBL. These layers are connected with weak stability or isothermal intermediate layers. This complex vertical lapse rate distribution results from the influence of the surrounding mountain–valley circulation on the previous day's CBL. The highest inversion layer usually is situated at the height of the previous day's CBL height. Figure 2 is an illustration of two different temperature and humidity profiles measured with tethered balloon after sunrise (a.s.) on 19 October 1988 (0945 LST) and again the formation of the

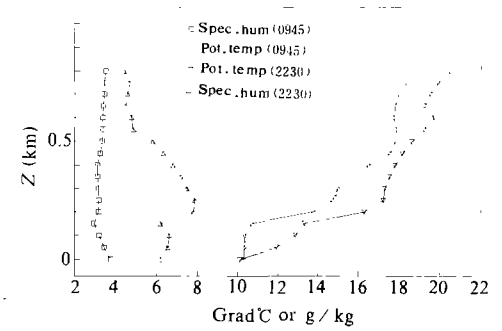

Fig. 2. Temperature (°C) and humidity (g / kg) profiles measured with tethered balloon after sunrise (a.s.) on 19 October 1988 (0945 LST) and during the formation of the nocturnal stable layer on 11 October 1990 (2230 LST). South Central Sofia: BAN site.

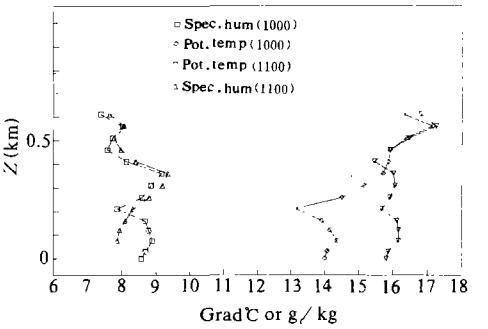

Fig. 3. Tethered balloon temperature and humidity profiles for 11 October 1991. South Central Sofia: BAN site.

nocturnal stable layer on 11 October 1990 (2230 LST). Similar profile data for 11 October 1991 are shown in Fig. 3, during our second study day. Unfortunately we did not take this kind of data on 21 September 1991.

2. *Measurements*

The measurement methods and equipment are described in detail by Donev et al. (1992a). The height of the aerosol layers and vertical temperature profiles after sunset, before and after sunrise have been observed aperiodically for several years in the Sofia Valley. These past measurements and our newly obtained results confirm that in case of calm weather there is a good coincidence in height between the inversion layers and the layers with strong lidar returns indicating high, homogeneous aerosol concentrations. For such stagnation type weather conditions the auto correlation functions of lidar returns give us approximate locations of h_0 and h_2 after sunrise. It is assumed that very stable air (inversions) tend to trap atmospheric aerosols while isothermal and weak lapse rate air allow aerosols to pass through. In this analysis of our experimental data we followed the approach used by Kaimal et al. (1976) and Caughey et al. (1979) which accounts for the relationship between the diurnal surface heat flux and the corresponding inversion rise. The vertical evolution of the inversion base h_0 and entrainment zone Δh compared to the surface heat fluxes $(\overline{w'\theta'})_s$ can be seen in Fig. 4 and Fig. 5. On September 21 the measured inversion base height grows from 120 m at 0640 LST to 700 m at 1300 LST, the end of the lider observations (case S). On October 11 it grows from 100 m (0815 LST) to 500 m (1230 LST) (case O). Several intervals of the boundary layer transition can be detected from these time series measurements:

Interval 1. First 30 min (S) and 60 min (O) a.s.: The surface heat flux is relatively small and the mixing layer is very thin h_0: 120 m; h_2: 270 m (S) and h_0: 100 m; h_2: 200 m (O) (the heights of the base and the top of the first inversion). This detail of h_0 and h_2 at the moment of sunrise is different from the usual definition but is very useful for making a smooth transition

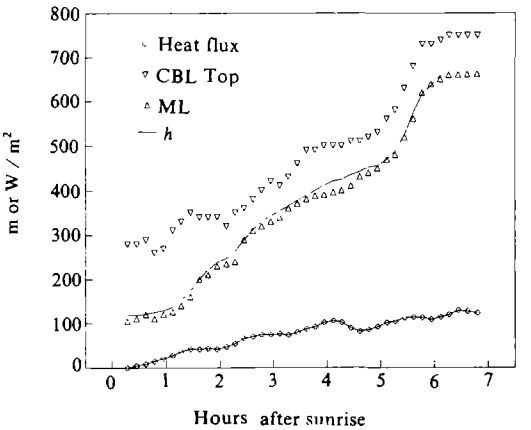

Fig. 4. The mixing layer height (ML) h_0, the top of the capping inversion, $h_0+\Delta h$ (CBL top), during the morning boundary layer transition on 21 September and the surface heat flux plotted as time after sunrise. Solid line is the smoothed approximation for h.

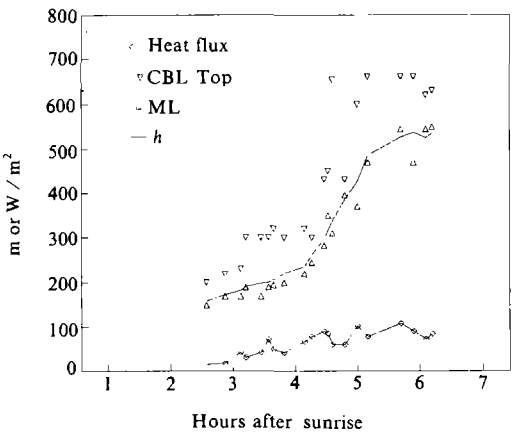

Fig. 5. As in Fig 4, but for 11 October.

from the nocturnal boundary layer definition to the CBL interpretation and allows the use of Deardorff's (1979) GSE model. The h_0 and h_2 heights are semi–constant for night and dawn and the classical definition for h_0 becomes valid when the first convective plums reach the bottom of these inversion layers after sunrise.

Interval 2. From 30 to 300 min (S) and from 60 to 270 min (O) a.s.: The mixing layer height, h_0, increases for both cases as the CBL grows due to earth surface heating. Several sub–stages of variable heat flux intensity can be distinguished but the CBL growth is closely correlated with jumps in heat flux intensity. "Synchronous" changes are seen in both Figs. 4 and 5 with an apparent phase lag between heat flux and CBL growth. There are also periods of relatively slow CBL growth in case S not associated with low heat flux. This appears to happen when the mixed layer height reaches the base heights of the first and the second intermediate inversion layers with bases at 150 and 350 m. The heights of the intermediate inversion layers were detected by lidar before sunrise as dense aerosol layers. The CBL stops growing for a certain time when these layers are reached. This phenomena is not as clear for the first inversion layer, but it is very obvious for the second inversion layer, when a stall in the CBL growth between 1045 to 1145 LST, (+3.5 to +4.5 h a.s.) is very noticeable. The growth of the mixing layer for this period is a function of the variability of heat flux, and lapse rates.

Interval 3. From 300 to 360 min (S) and from 270 to 330 min (O) a.s.: This interval is characterized by a sharp increase in the growth of the mixing layer height in the residual layers (very small lapse rates).

Interval 4. 6 h a.s.: The maximum mixing layer height is reached (about 700 m for case S and 500 m for case O).

IV. A METHOD FOR VERTICAL STABILITY AND MIXING HEIGHT ESTIMATION

Models of mixing layer growth are particularly sensitive to lapse rate γ_e. Hence, an accurate knowledge of γ_e is required for good predictions of CBL growth. Bulgarian aerological soundings do not provide reliable accuracy in the first three or four hundred meters and tethered balloon sondes are technically difficult on a routine basis and they have problems associated with their use during the time development of vertical stability changes. It is much easier to observe the evolution of the CBL using remote sensing (lidar or acoustic sounding). Our goal here is to construct a simple diagnostic model of vertical stability using lidar observed mixing layer and entrainment zone together with surface heat flux measurements.

1. *Determining Lapse Rate from Lidar and Heat Flux*

As input in this procedure we use either the values of h_0, h_2 and $(\overline{w'\theta'})_s$, or $\Delta h = h_2 - h_0$ and $h = h_0 + \beta h_0$, where $\beta = \Delta h_1 / h_0 \propto Ri^{9/16}$ is chosen following Fernando (1986). This approach for h does not ensure a maximum negative heat flux value, hence it is considered only a first guess. The lidar measurements provide approximate estimations of average h_0, h_2 and their time derivatives. This lapse rate diagnostic is useful in the Sofia Valley only when the horizontal winds are calm or very weak. An iterative procedure, described below is used to obtain both γ_e and the intensity of the temperature inversion $\Delta\theta$, capping the mixed layer. These quantities are critical in all mixing height and air quality models.

A first approximation for the lapse rate aloft: γ_e', (square symbols in Figs. 6 and 7), is made with $A = 0.2$ and neglecting the mean vertical velocity at the top of the mixed layer in Eqs. (1) and (2) or by using only the second part of Eq. (1) (rhomb symbols in Figs. 6 and 7). According to the main physical limitation in this paper the total potential temperature jump between h_0 and h_2 consists of a steady contribution, $\Delta\theta_0$, and a variable contribution $\gamma_e(h_2 - h)$. Next, the first approximation γ_e is substituted into (6), Deardorff's, (1979) GSE model, to extract $\Delta\theta'$ which gives the best fit to the known h_0 and h_2. The next step is to estimate the first

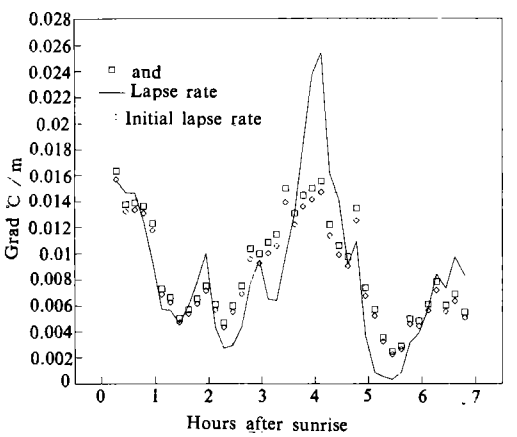

Fig. 6. First and established approximation of the lapse rate in the stable air aloft for 21 September.

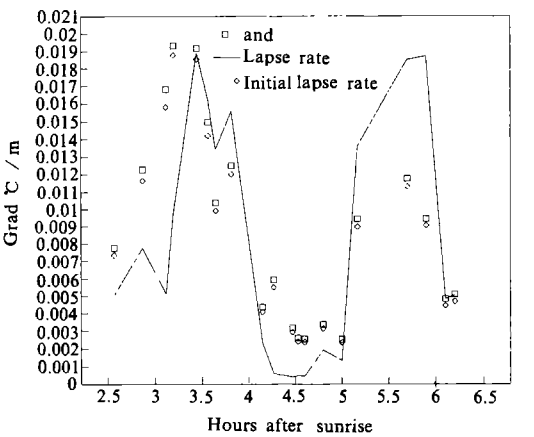

Fig. 7. As in Fig. 6, but for 11 October.

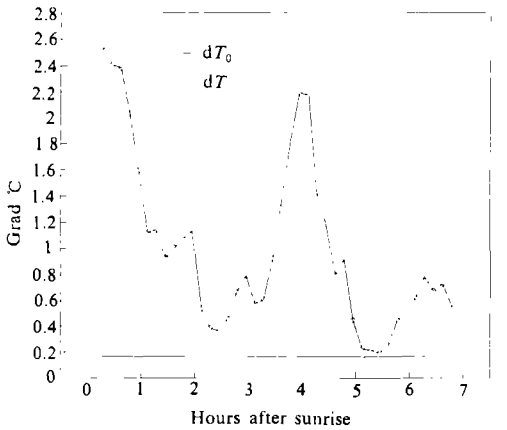

Fig. 8. Diagnostic output of the intensity of the capping inversion and constant potential temperature jump at h for 21 September 1991.

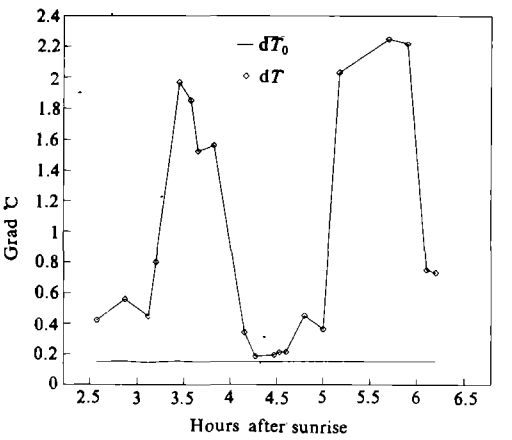

Fig. 9. As in Fig. 8, but for 11 October.

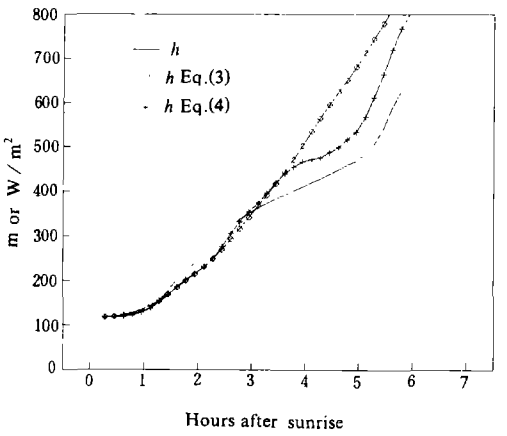

Fig. 10. Comparison of the modelled mixed layer growth and measured h, if calculated γ_e and $\Delta\theta$ are substituted in the right hand side of Eqs. (3) and (4) for 21 September using: $A_1=0.2$, $C_1=C_2=2$, $A_2=0.35$ and $A_2'=0.03$.

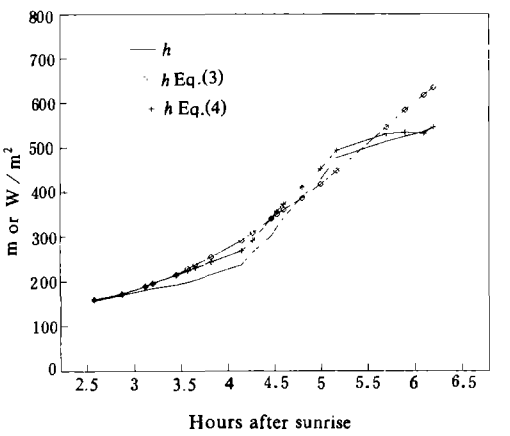

Fig. 11. As in Fig. 10, but for 11 October.

approximation for $\Delta\theta_0'$ as the average of $\Delta\theta'-\gamma_e'(h_2-h)$ and then employ this relation again $\gamma_e''=(\Delta\theta'-\Delta\theta_0')/(h_2-h)$ to obtain the second approximation for the lapse rate γ_e. From Eq.(6) we receive the second approximation for $\Delta\theta$. These steps are repeated iteratively until stable estimates of γ_e (Figs. 6 and 7), $\Delta\theta$ and $\Delta\theta_0=$ const. are generated (Figs. 8 and 9).

2. *Verification and Test of the Obtained γ_e and $\Delta\theta_0$*

In order to verify this method, the available measured vertical temperature distribution is used: tethered balloon measurements on 11 October and approximate estimations of the

temperature profile 2 h a.s. on 21 September from the standard Sofia aerological sounding. Figure 3 gives the tethered balloon temperature and humidity profile results at intervals of 50 m in the course of ascending 0930 to 1020 LST and descending 1030 to 1130 LST up to 600 m. The ascending and descending time lags make the precise interpretation of lapse rate difficult but there are some conclusions from these profiles. At 1000 (+3.7 h a.s.) there is a strong inversion layer between 200 and 300 m with a temperature jump of 1.5°C. This is in good agreement with the model diagnostic displayed in Fig. 9. The descending profile (1030 to 1130 LST) coincides with the sharp increase in the mixing layer height (Fig. 5). There were no noticeable inversion layers below 400 m (the measured mixing layer height at 1100 LST). The small temperature inversion aloft also agrees with the diagnostic model temperature jump minimum. On 21 September (Figs. 8 and 4), the aerosol layers are at 150, 350 and 700 m as detected with lidar a few minutes before sunrise. The Sofia aerological sounding at 0800 LST confirms the highest inversion layer and indirectly the second as indicated by an increase in wind speeds above 350 m. The Sofia aerological sounding at 0200 LST confirms the formation of these two inversion layers.

To test the diagnosing output for γ_e and $\Delta\theta_0$ in Figs. 10 and 11 we show the calculated mixed layer growth obtained if calculated γ_e and $\Delta\theta_0$ are substituted in the right hand side of Eqs. 3 and 4. This reasonably good fit of calculated to measured h corresponds to: $A_1=0.2$, $C_1=C_2=2$, $A_2=0.35$ and $A_2'=0.03$. The deviation from the measured heights in Fig. 10 after +3 h a.s. can be explained with departure from the pure convective conditions and appearance of dynamic factors for the mixed layer growth. The selection of the parameters follows from the comparison between different model predictions in Arya and Byun (1987).

V. CONCLUSIONS

(1) It was known that in case of calm weather, a strong temperature inversion exists near the surface in Sofia Valley. Excluding the surface radiative measure, this inversion base is about 150 m high in September and diminishes to 50 m in late November. There is one or more layered inversion layers stacked up to the previous day's CBL height, connected with weak stability or isothermal interfacial layers. The highest inversion layer is usually situated at the height of the previous day's CBL height.

(2) During the CBL development in calm wind conditions, jumps in mixing layer height are correlated with surface heat flux maximums. There are intermittent periods of relatively slow mixing layer development apparently slowed when the mixed layer height reaches the heights of the interfacial inversion layers. These interfacial inversion layers can be detected before sunrise as dense aerosol layers using lidar.

(3) Standard aerological soundings do not give us enough accuracy in the first three or four hundred meters, and tethered balloon sondes are not ideal. A simple procedure for diagnosing vertical stability is presented which uses lidar observed mixing layer evolution entrainment zone thickness together with surface heat flux measurements: using values of h_0, h_2 and $(\overline{w'\theta'})_s$ to generate γ_e and the intensity of the capping temperature inversion. These quantities are required for the air quality models. The main limitation of the diagnostic method is the proposal for the invariability of the $\Delta\theta_0$. The results are encouraging under convective conditions, because there is relatively good agreement between the experimental data used for verification and there is reasonably good fit of calculated from Eqs. 3 and 4 to measured h with close to the

generally accepted constants.

REFERENCES

Arya, S. P. S. and Byun, D. W. (1987), Rate equations for the planetary boundary layer depth (urban vs rural), *Modeling the Urban Boundary Layer*, Amer. Meteor. Soc., pp.215—251.

Boers, R. and Eloranta, E. W. (1985), Lidar measurements of the atmospheric entrainment zone and the potential temperature jump across the top of the mixed layer, *Boundary Layer Meteor.*, **34:** 357—375.

Boers, R., Eloranta, E. W. and Coulter, R. L. (1984), Lidar observations of mixed layer dynamics: Tests of parameterization entrainment models of mixed layer growth rate, *J. Climate and Appl. Meteor.*, **23:** 247—266.

Carson, D. J. (1973), The development of a dry inversion-capped convective unstable boundary layer, *Quart. J. Roy. Meteor. Soc.*, **99**: 450—467.

Caughey, S. J., Wyngaard, J. C. and Kaimal, J. C. (1979), Turbulence in the evolving stable boundary layer, *J. Atmos. Sci.*, **36:** 1041—1052.

Deardorff, J. W. (1974), Three-dimensional numerical study of the height and mean structure of a heated planetary boundary layer, *Boundary Layer Meteor.*, **7:** 81—106.

Deardorff, J. W. (1979), Prediction of convective mixed layer entrainment for realistic capping inversion structure, *J. Atmos. Sci.*, **36:** 424—436.

Deardorff, J. W. (1980), Progress in understanding entrainment at the top of a mixed layer, *Workshop on the Planetary Boundary Layer*, Amer. Meteor. Soc., Boston, MA, pp.36—66.

Donev, E., Ivanov, D., Kolev, I., Kaprielov, B., Parvanov, O. and Zeller, K. (1992a), Comparisons between lidar observed stratified layer and surface vertical heat and humidity fluxes, *Bulgarian J. Meteor. and Hydrology*, **3(2):** 101—106.

Donev, E., Zeller, K. and Kolev, I. (1992b), The morning boundary layer transition in response to the surface heat flux, *10th Symposium on Turbulence and Diffusion*, Sept. 29—Oct. 2, 1992, Portland, USA, pp. 242—243.

Driedonks, E. G. W. (1982), Models and observations of the growth of the atmospheric boundary layer, *Boundary Layer Meteor.*, **23**: 283—306.

Fernando, H. J. S. (1986), On buoyancy transfer across an entrainment interface, *Boundary Layer Meteor.*, **34**: 171—176.

Kaimal, J. C., Wyngaard, J. C., Haugen, D. A., Cote, O. R., Izumi, Y., Caughey, S. J. and Readings, C. J. (1976), Turbulence structure in the convective boundary layer, *J. Atmos. Sci.*, **33**: 2152—2169.

Lilly, D. K. (1968), Models of cloud-topped mixed layers under a strong inversion, *Quart. J. Roy. Meteor. Soc.*, **94**: 292—309.

Tennekes, H. (1973), A model for the dynamics of the inversion above a convective boundary layer, *J. Atmos. Sci.*, **30**: 558—567.

Tennekes, H. and Driedonks, A. G. M. (1981), Basic entrainment equations for the atmospheric boundary layer, *Boundary Layer Meteor.*, **20:** 516—531.

Wyngaard, J. C. (1983), Lectures on a planetary boundary layer, *Mesoscale Meteorology——Theories, Observations and Models*, D. Reidel, Dordrecht, Holland.

Zeman, O. and Tennekes, H. (1977), Parameterization of the turbulent energy budget at the top of the daytime atmospheric boundary layer, *J. Atmos. Sci.*, **34:** 111—123.

Zilitinkevich, S. S. (1975), Comments on a model for the dynamics of the inversion above a convective boundary layer, *J. Atmos. Sci.*, **32**: 991—992.